Available online at website: https://journal.bcrec.id/index.php/bcrec

Bulletin of Chemical Reaction Engineering & Catalysis, 19 (3) 2024, 470-479

Research Article

Fabrication of Zn and Ti-loaded Carbon-silica Composite Derived from Gelatin Template for the Photodegradation of Methylene Blue

Maria Ulfa*, Ika Uswatun Hasanah, Ida Setiarini

Chemistry Education Study Program, Faculty of Teacher Training and Education, Sebelas Maret University, Jl. Ir. Sutami 36A, Surakarta 57126, Indonesia.

Received: 13th August 2024; Revised: 10th September 2024; Accepted: 12th September 2024
Available online: 14th September 2024; Published regularly: October 2024

Abstract

Carbon-silica nanocomposites (CSNs) from gelatin as a carbon source and natural template and TEOS as a silica source have been successfully synthesized and impregnated into ZnO and TiO_2 photocatalysts. The structural, morphological, and textural properties and photocatalytic activity for methylene blue degradation of TiO_2/CSNs and ZnO/CSNs were investigated. XRD data revealed that TiO_2/CSNs and ZnO/CSNs had different structural characteristics with similar crystallinity. FTIR spectra demonstrated the presence of Zn–O and Ti–OC bonds, respectively, at about 500-450 cm^{-1} and 1500 cm^{-1}. The morphological surface exhibited stacked tubular shapes of TiO_2/CSNs and ZnO/CSNs with the primary elements of Ti, Zn, Si, C, and O. The nitrogen adsorption-desorption curves revealed both micropores and mesopores of TiO_2/CSNs and ZnO/CSNs where the surface area reduced due to the blocking pore after impregnation. Moreover, ZnO/CSNs verified a higher degradation percentage against methylene blue than that of TiO_2/CSNs.

Keywords: carbon-silica, composite, gelatin, photodegradation, Zinc, Titania, Methylene blue

How to Cite: M. Ulfa, I. U. Hasanah, I. Setiarini (2024). Fabrication of Zn and Ti-loaded Carbon-silica Composite Derived from Gelatin Template for the Photodegradation of Methylene Blue. *Bulletin of Chemical Reaction Engineering & Catalysis*, 19 (3), 470-479 (doi: 10.9767/bcrec.20193)

Permalink/DOI: https://doi.org/10.9767/bcrec.20193

1. Introduction

Methylene blue ($C_{16}H_{18}C_lN_3S$) is a toxic aromatic hydrocarbon compound generally used as a dye for textiles, paper, cosmetics, and office equipment [1,2]. Unfortunately, this compound only uses around 5% of the coloring, while the remaining 95% is discarded as waste [3]. In large concentrations, methylene blue waste can enhance COD (Chemical Oxygen Demand), which can damage the environmental ecosystem . To remove pollutants of methylene blue dye waste, several technologies have been applied, including coagulation, flocculation, Fenton, ozonation, photocatalysis, adsorption, and a combination of ozonation with photocatalysis [4,5]. Among these methods, photocatalysis is considered the most efficient and superior in degrading dyes since it can transform organic compounds into more straightforward and safer components for the environment. This process employs energy originating from UV light or sunlight to activate the photocatalysis process on the surface of semiconductor materials (photocatalyst), which will produce hydroxyl radicals (OH-) as organic pollutant degraders [6–8]. Hydroxyl radicals have high reactivity, so if the number of hydroxyl radicals increases, more dye will be degraded. Two semiconductor materials extensively used as photocatalysts are TiO_2 and ZnO [9–12].

Titanium dioxide (TiO_2) is a metal oxide semiconductor with a bandgap energy of 3.2 eV for the anatase phase that is nontoxic and chemically and structurally stable [13]. TiO_2 photocatalysts have been well-known for their applications, one of which is the degradation of pollutants.

* Corresponding Author.
Email: ulfa.maria2015@gmail.com (M. Ulfa)

Meanwhile, ZnO is inert, abundantly available in nature, nontoxic, inexpensive to manufacture, environmentally friendly, and can be made under standard reaction conditions, so it is often used as a photocatalyst in photodegradation [11]. The bandgap energy of ZnO is slightly lower than that of TiO_2, namely 3.17 eV. Prior research reported that ZnO nanoparticles could degrade 50 ppm of methylene blue dye solution up to 92.34% [14].

However, semiconductor metal oxides such as ZnO and TiO_2 tend to experience agglomeration, which can reduce their photocatalytic performance [15,16]. Besides, the high level of agglomeration causes a photocatalytic reaction that requires a lot of semiconductors as active centers, which requires high costs. Therefore, efforts to minimize catalyst agglomeration are often carried out by dispersing the catalyst in a porous matrix such as silica, carbon, metal, or polymer [17–19]. Carbon-silica composite is a porous material that is rarely used as a catalyst matrix because of the complexity of the manufacturing process [5,20,21].

Carbon-silica composites are materials consisting of carbon and silica, where the physicochemical properties of carbon combined with the unique characteristics of silica produce materials with extraordinary features such as high thermal stability, large surface area, and regular structure and texture [22,23]. The properties cause carbon-silica composites to be included in the category of promising materials in various applications, especially as matrix/catalyst supports, fillers, absorbers, adsorbents, filters, and solar absorbers. Carbon-silica in previous research has been made with various chemicals or polymers such as hydrocarbon gas (C_3H_6), (poly)furfural alcohol (PFA), furfuryl alcohol (plus acid catalyst), and dichloromethane as carbon sources [24,25].

However, many carbon sources are expensive and potentially toxic and produce toxic by-products during carbonization. Therefore, recent studies have focused on synthesizing carbon-silica composites from economical, abundant, naturally derived, and nontoxic sources. Recent research demonstrated that the use of pyrolysis oil from cellulose waste could yield carbon-silica materials with high porosity. Sucrose has also been used as a safer and more sustainable carbon source. Still, as a high-quality food product, it requires high costs in the production of chemicals, raw materials, and fuel. In particular, gelatin is a waste product from the hydrolysis of animal skin and bone that is cheap and safe and can be used as an effective carbon source for making carbon silica [26,27]. Besides, gelatin in several previous studies has been successfully employed not only as a carbon source but also as a natural template.

This present study was novel, reporting the synthesis of carbon-silica nanocomposites from gelatin as a carbon source and natural template and tetraethyl-orthosilicate (TEOS) as a silica source with a one-pot method. The resulting carbon-silica nanocomposite was employed as a supporting material for ZnO and TiO_2 photocatalysts by applying a simple wet impregnation method. Thus, this study further investigated the properties of ZnO- and TiO_2-impregnated carbon-silica nanocomposites, including structural, morphological, and textural. Moreover, ZnO-impregnated and TiO_2-impregnated carbon-silica nanocomposites were applied as the photocatalyst for degrading methylene blue. Hence, this study observed the photocatalytic activities of the two samples for degrading methylene blue.

2. Methods

2.1 Materials

The materials were HCl 37% (MW = 36.5 g/mol), distilled water (MW = 18 g/mol), pluronic triblock copolymer P123 (MW = 5750 g/mol), commercial gelatin (MW = 90,000 g/mol), Tetraethyl orthosilicate (TEOS) (MW = 208.33 g/mol), Tetraethyl ortho titanate (TEOT) (MW = 228.109 g/mol), $Zn((CH_3COO)_2.2H_2O)$, n-hexane pro analysis (MW = 86.178 g/mol), and Methylene Blue (MW = 319.85 g/mol). All reagents were purchased from Sigma Aldrich.

2.2 Synthesis of Carbon-silica Nanocomposites (CSNs)

19.5 mL of 37% HCl was diluted in 127 mL of distilled water. After that, 4 grams of P123 and 0.04 grams of gelatin were mixed with the HCl solution by stirring at a speed of 500 rpm at 40 ^oC for 3 hours, followed by 9.24 mL of TEOS. The mixture was put into an autoclave reactor for the hydrothermal reaction. The autoclave was heated at 90 ^oC for 24 hours, and the result was filtered and dried. The resulting white powder was then calcined in a furnace at 550 ^oC for 5 hours until carbon-silica nanocomposite powder (CSNs) was formed.

2.3 Synthesis of ZnO/CSNs

The 5% (w/w) of Zn is impregnated on CSNs as the support from precursor. The impregnation of ZnO in CSNs was done by separately dissolving $Zn((CH_3COO)_2.2H_2O)$ (Zn precursor) in 20 mL of water followed by homogenization using stirrer magnetic 5 h at room temperature in 150 rpm. The results were then dried 100 ^oC for 24 h then calcined at 550 ^oC for 5 hours. The resulting samples were named ZnO/CSNs.

2.4 Synthesis of TiO_2/CSNs.

The 5% (w/w) of Zn is impregnated on CSNs as the support from precursor. The impregnation

of TiO_2 in CSNs was done by separately dissolving Tetraethyl ortho titanate (TEOT) (Ti precursor) in 20 mL of n-hexane followed by homogenization using stirrer magnetic 5 h at room temperature in 150 rpm. The results were then dried 100 °C for 24 h then calcined at 550 °C for 5 hours. The resulting samples were named TiO_2/CSNs.

2.5 Characterizations

X-ray diffraction (XRD) by Pananalytica Version PW3050/60 instrument with Cu-Kα radiation (1.5418 Å) with an angle range of 10°-80° was performed to determine the crystal size and crystallinity. Fourier Transform Infrared (FTIR) by Spectrum GX FT-IR (Perkin Elmer) with a potassium bromide (KBr) beam splitter was employed to observe the functional groups. Scanning Electron Microscopy-Energy Dispersive X-ray (SEM-EDX) by Tescan Mira3 SEM-Czechia SEM was applied to investigate the morphology and diameter of the particles. Bruneuer Emmet Teller (BET) method was used to identify surface area, pore volume, and pore diameter using BET by Quantacrome Nova 1200e. UV-Vis DRS (Diffuse Reflectance Spectroscopy) was utilized to estimate the bandgap energy using a double-beam spectrophotometer (UV-1800, Shimadzu) in the 200-900 nm range.

2.6 Photodegradation of Methylene Blue

The photodegradation activity of the two catalysts was evaluated by measuring the degradation of Methylene Blue in wastewater solution under UV light radiation. The experiment was done in a photocatalytic reactor. Before the experiment, 50 mg of photocatalyst was added to 200 mL of methylene blue solution (5 mg/L) by stirring for 30 minutes in the dark condition to reach adsorption-desorption equilibrium. Then, the mixture was placed vertically under a 300 W Xenon lamp equipped with an optical transmission filter (λ = 365 nm). After that, 10 mL of the irradiated mixture was collected at fixed irradiation times (10, 20, 30, 40, 50, 60, 70, 80, and 90 min) and centrifuged to remove the photocatalyst. The methylene blue concentrations before and after irradiation were determined by measuring the absorbances at a wavelength of 665 nm with a UV-Vis spectrophotometer (Shimadzu UV-3600).

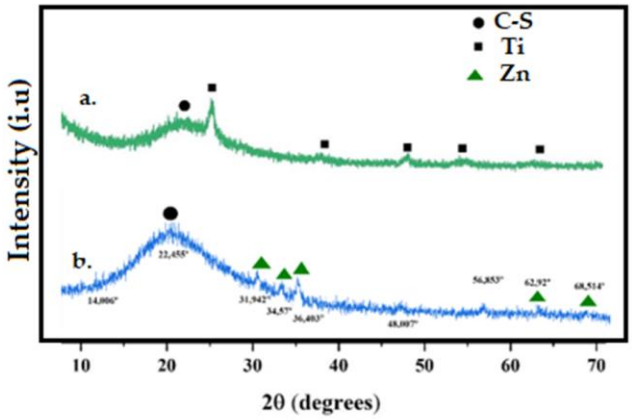

Figure 1. XRD patterns of TiO_2/CSNs and ZnO/CSNs

3. Results and Discussion

Figure 1 depicts the XRD patterns of the prepared photocatalysts. The XRD patterns showed a large hump at 2θ = 20-26° and 42.6°, indicating the carbon's amorphous nature. They were indexed to the (002) and (101) planes of the hexagonal graphite lattice corresponding to JCPDS card number 41-1487 [28,29]. Besides, all spectra showed a peak at 22°, indicating silica's cristobalite structure [30]. In Zn/CSNs, other prominent peaks were revealed at 2θ = 31°, 34°, 36°, 47°, 56°, 62°, 66°, 67°, and 69°, corresponding to the crystalline hexagonal structure of ZnO assigned to planes (100), (002), and (101). Meanwhile, the XRD patterns of TiO_2/CSNs lacked significant peaks, possibly due to TiO_2 concentrations below the XRD instrument's detection range. It is also suggested that the TiO_2 crystallites (Equations 1-2) formed were less than 13 nm (Table 1), indicating highly dispersed. This results in intensities of the peaks responsible for the typical attributes of the diffraction patterns for the anatase structure at approximately 25.3°, 37.0°, 38.0°, 38.5°, and 48.0° (JCPDS 21-1272) [31,32]. Furthermore, although the XRD patterns of all samples revealed the different structural properties of TiO_2 and ZnO, their crystallinity (Equation 1) remained consistent.

The crystallinity (%) (Equation 1) of the sample can also be calculated through X-ray Diffraction characterization data using the following formula:

$$Crystallinity = \frac{cryst.peak\ area}{cryst.and\ amorph.peak\ areas} x100\% \quad (1)$$

Calculating crystal size is done using the Debye Scherrer formula as in the equation below:

$$D = \frac{0.9\,\lambda}{B.cos\,\theta} \quad (2)$$

Table 1 Crystallite size (D) and crystallinity of catalysts by XRD

Sample	Crystallinity (%)	D (nm)
ZnO/CSNs	43.390	12.64
TiO_2/CSNs	43.558	27.91

D is the crystallite size (Equation 2) in Å, λ is the wavelength used in the XRD test which is 1.540 Å, and *B* is the half-peak width in radians. θ is the angular position of the peak formation. The XRD results also show the FWHM to determine the *B* value (rad).

Figure 2 displays the FT-IR spectra of TiO_2/CSNs and ZnO/CSNs. The spectra revealed silica bands at 3500, 1060, and 800 cm^{-1}, indicating OH stretching, asymmetric Si–O–Si bond stretching, and SiO_4 tetrahedron ring, respectively [33,34]. The band at 1620 cm^{-1} was attributed to the stretching of C=C [35]. The absorption band at 1456 cm^{-1} was associated with C–H from the methylene group, while the band at 1582 cm^{-1} denoted the C=C aromatic skeletal vibrations [36]. The resulting IR spectra show several significant differences between samples containing ZnO and TiO_2 metal oxides. The sharp peak in the ZnO/CSNs spectrum at 500-450 cm^{-1} was related to the presence of metal oxide stretching vibrations from the Zn–O bond [37]. Meanwhile, in the TiO_2/CSNs spectrum, a peak at about 1500 cm^{-1} was a typical characteristic of Ti–O–C [38]. This study found that aromatic structures were produced during high-temperature treatment, and Ti and Zn elements were successfully incorporated into the carbon-silica framework. FTIR results were supported by EDX data.

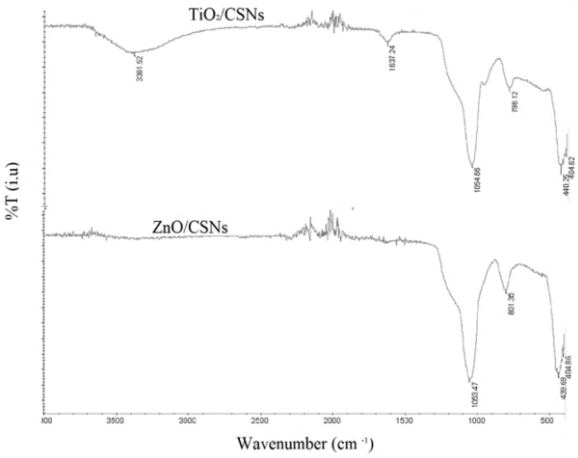

Figure 2. FTIR spectra of TiO_2/CSNs and ZnO/CSNs

Figure 3 depicts the SEM images, EDX spectra, and particle size distribution of the TiO_2/CSNs and ZnO/CSNs composites. The results indicate that the ZnO and TiO_2 phase was successfully integrated into the carbon-silica nanocomposite support. The EDX analysis (Figures 3c and 3d and Table 2) confirmed this conclusion in which Ti, Zn, Si, C, and O became the primary constituents in the samples. This approach also examined the C/Si = 1.32-1.38 ratio, which is consistent with conventional carbon-silica nanocomposite values. Besides, as seen in Figure 3a, the TiO_2 is uniformly distributed over the carbon-silica surface (not detectable on SEM due to the small percentages of Ti and Zn, which was less than 5% (Table 2). Further, the SEM images (Figures 3a and 3b) illustrate a type of composite in which carbon-silica presents its characteristic stacked tubular morphology.

The diameter of the support decreases after metal impregnation. This is because the Ti and Zn particles impregnated into the Mesoporous Silica experience interatomic attraction and form smaller particle sizes. The addition of gelatin affects the formation of silica morphology. Gelatin can activate the condensation process of silica precursors through hydrogen bonds or electrostatic interactions of the NH_3^+ or COO^- groups on the peptide chain with silanol species. Gelatin also plays a role in the growth of silica nuclei to the aggregation of silica particles which is an aggregation process that plays an important role in the formation of mesoporous material morphology. Gelatin can make materials more porous, because it can form more surfactant micelles and micelles can create more pores, thereby increasing the surface area and total pore volume.

Table 2. Elemental compositions of TiO_2/CSNs and ZnO/CSNs observed by EDX

Photocatalyst	Diameter, (nm)	Elemental Composition Analysis (%wt)*				
		C	O	Si	Ti	Zn
CSNs	524.95	9.4	49.03	41.57	-	-
TiO_2/CSNs	388.61	28.81	45.72	21.76	3.00	-
ZnO/CSNs	434.76	28.05	49.47	20.22	-	2.26

*The elemental compositions were measured using Energy-Dispersive X-ray Spectroscopy (EDX). The EDX tests were carried out using a scanning electron microscope (SEM) equipped with an EDX detector. To guarantee that the surface composition was represented, the samples were scanned in multiple locations. Elements were quantified by integrating the distinctive X-ray peaks for each element and normalising to the overall number of elements found. The accuracy of the analysis was ensured by using ZAF (atomic number, absorption, and fluorescence) correction factors during the quantification process.

Figure 4 presents the nitrogen adsorption-desorption isotherms and pore size distribution of TiO_2/CSNs and ZnO/CSNs. The nitrogen adsorption-desorption curves show that all samples exhibited a combination of types I and IV isotherms, suggesting the existence of both micropores and mesopores in the structure. TiO_2/CSNs and ZnO/CSNs inherited mesoporosity characteristics from the parent CSNs, with the surface area decreased (Table 3) due to the blocking pore after impregnation.

ZnO has strong electron bond energy and high electron bond energy. Zn^{2+} in ZnO has an orbital diagram of $1s^2\ 2s^2\ 2p^6\ 3s^2\ 3p^6\ 3d^{10}$ where the d orbitals are full. This causes a low level of ZnO agglomeration when ZnO is impregnated into

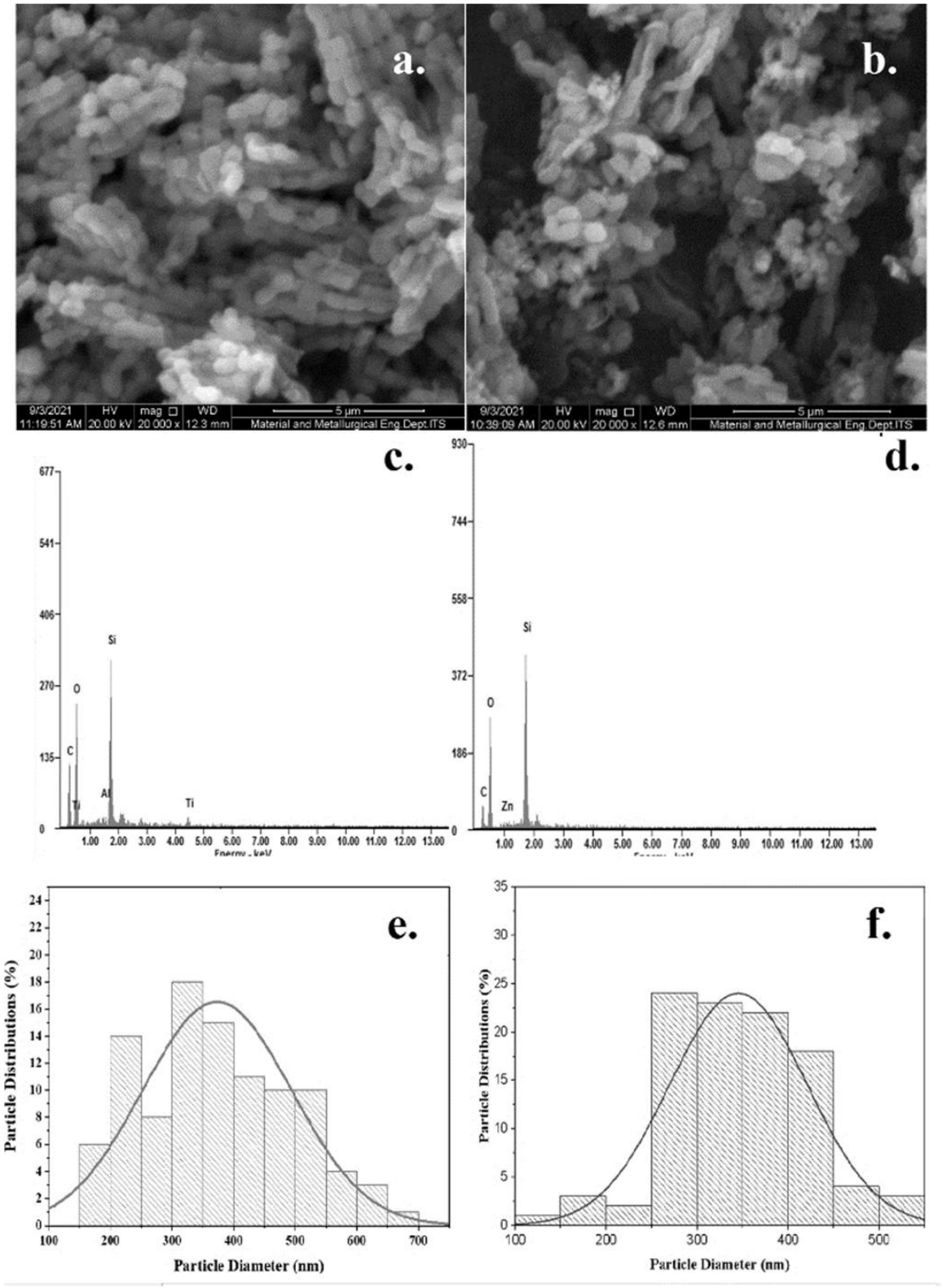

Figure 3. SEM images, EDX spectra, and particle distributions of TiO_2/CSNs (a, c, and e) and ZnO/CSNs (b, d, and f)

CSNs. Further, this causes a smaller level of surface area reduction compared to TiO_2 because Zn tends not to easily attract electrons from other elements such as oxygen or Zn fellow. This condition prevents massive agglomeration from occurring, which causes only a small portion of the CSN's surface to be covered with ZnO agglomerates.

Figures 5-6 shows the percentages dan psectra of methylene blue photodegradation by TiO_2/CSNs and ZnO/CSNs with various irradiation times. ZnO/CSNs has the ability to degrade methylene blue by 92.80%, TiO_2/CSNs by 77.17%, while CSNs is only 61.50%. This proves that CSNs that have been added with active metals Zn and Ti have higher and better photocatalytic activity. Further, the figure exhibits that ZnO/CSNs resulted in a higher degradation percentage than that of TiO_2/CSNs. This can be explained based on the type of metal on the photocatalyst surface. Zn metal in the form of Zn^{2+} on the carbon-silica surface is an active site

Table 3. Textural properties of TiO_2/CSNs and ZnO/CSNs. a = Surface area of material resulting from BET instrument; b = Pore volume determined by BJH method; c = Pore diameter (D) determined by BJH method; d = The photodegradation efficiency of MB by UV-VIS

Sample Type	CSNs	ZnO/CSNs	TiO_2/CSNs
[a]S_{BET} (m^2/g)	500.800	390.435	369.631
[b]Pore volume (cm^3/g)	0.706	0.600	0.639
[c]Pore diameter (Å)	28.161	30.740	34.609
[d]% Efficiency	61.500	92.800	77.170

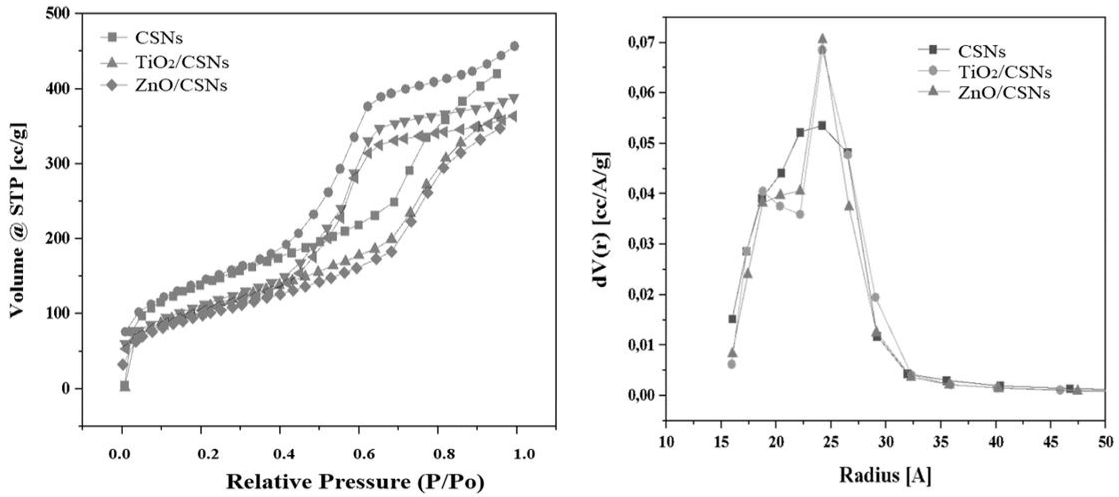

Figure 4. Nitrogen adsorption-desorption isotherms and pore size distribution of TiO_2/CSNs and ZnO/CSNs

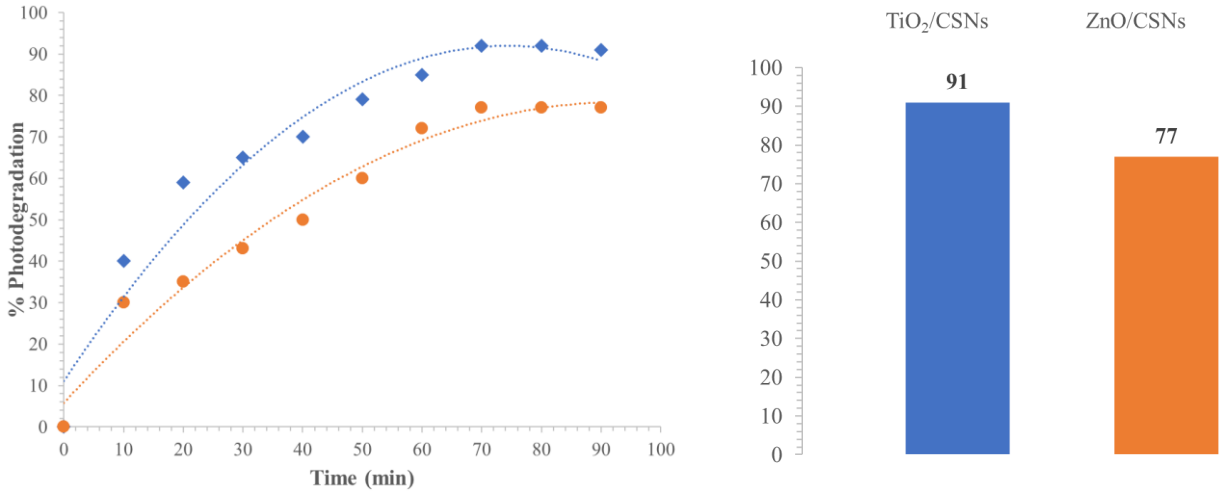

Figure 5. Methylene blue photodegradation by TiO_2/CSNs and ZnO/CSNs

that emits electrons supported by the surface area of the support material. This condition supports the adsorption of methylene blue on the ZnO surface and increases the direct oxidation of methylene blue. Degradation is expected to occur on the surface of the material. The carbon-silica composition of ZnO/CSNS can contribute to absorption through electrostatic interactions, so total photodegradation was higher than that of TiO_2/CSNs. Among the catalyst samples that have been synthesized, the highest photocatalytic efficiency achieved by ZnO/CSNs in minutes is higher than the average for pure ZnO and TiO_2 from previous references (Table 3). This is new insight into the importance of support materials such as carbon-silica based CSNs, which have great potential in air treatment.

The mechanism of the methylene blue degradation reaction on TiO_2/CSNs and ZnO/CSNs photocatalysts under light irradiation can be written as follows:

$$TiO_2 + hv \rightarrow TiO_2\ (e^- + h^+) \quad (3)$$
$$ZnO + hv \rightarrow ZnO\ (e^- + h^+) \quad (4)$$
$$OH^- + h^+ \rightarrow OH^{\cdot} \quad (5)$$
$$H_2O + h^+ \rightarrow OH^{\cdot} + H^+ \quad (6)$$
$$\cdot OH + \text{Methylene blue} \rightarrow CO_2 + H_2O \quad (7)$$
$$\text{Methylene blue} + e^- \rightarrow CO_2 + H_2O \quad (6)$$

When TiO_2/CSNs and ZnO/CSNs photocatalysts absorb photons from a light source with energy equal to or greater than their band gap energy, then the electrons in TiO_2 and ZnO are excited from the valence band to the conduction band, producing electron-hole pairs. In which, e^- dan h^+ are respectively electrons in the conduction band and holes in the valence band. Both of these entities can migrate to the surface of TiO_2/CSNs and ZnO/CSNs and enters into a redox reaction

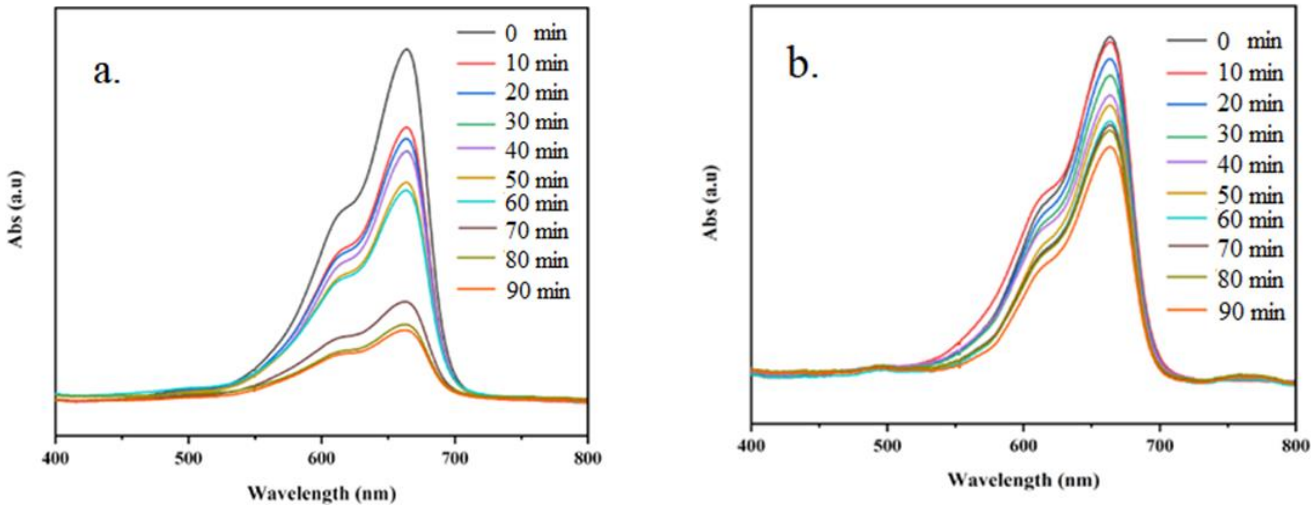

Figure 6. UV-Vis spectrum of methylene blue solution degraded by a. ZnO/CSNs and b. TiO_2/CSNs

Table 4. Comparation study with previous research

Sample	%Efficiency	Condition	Ref
TiO_2 rutile	78	Irradiation 240 min	[39]
ZnO nanosheets	99	pH = 2, MB 40 mg/L, catalyst 0.1 g. UV light 500 W Hg lamp irradiation 50 min	[40]
ZnO (with sulfur)	73	Irradiation 5 h, MB solution 1 M	[41]
Pure ZnO	59	using a 200W Xe lamp (light intensity=25 mW/cm^2), irradiation 180 min	[42]
TiO_2 (with inulin)	90	50 mL of MB, 0.01 catalyst, irradiation strength 17.0 µW/cm^2 , 150 min	[43]
TiO_2	80	Solgel method, UV lamp 366 nm, 30 W, 0.2 g of photocatalyst, 500 mL of MB solution (20 mg/L	[44]
TiO_2 microsphere	82	UV illumination 375 W mercury lamp, 0.02 g of catalyst 100 mL MB 10 mg/L , irradiation 180 min	[45]
TiO_2 P25	40	Partice size 25 µm, irradiation 40 min	[31]
TiO_2/CSNs	91	50 mg catalyst, 200 mL MB 5 mg/L, irradiated 90 min	This work
ZnO/CSNs	77		

with organic pollutants, in this case, methylene blue, on the surface. Holes will react with H_2O or OH^- to generate hydroxyl radicals (•OH). These radicals are powerful oxidizing agents and the main oxidizers in the photocatalytic oxidation process of methylene blue to carbon dioxide, water, and other mineralized products. Meanwhile, electrons (e^-) will react with methylene blue to produce reduction products, namely CO_2 and H_2O.

4. Conclusion

Carbon-silica nanocomposites (CSNs) from gelatin as a carbon source and natural template and TEOS as a silica source have been successfully synthesized with a one-pot method. Carbon-silica nanocomposites were employed as a supporting material for ZnO and TiO2 photocatalysts by applying a simple wet impregnation method. TiO_2/CSNs and ZnO/CSNs exhibited different structural characteristics with similar crystallinity. The typical characteristics of ZnO- and TiO_2-impregnated samples were revealed with the presence of Zn-O and Ti-OC bonds, respectively, at about 500-450 cm-1 and 1500 cm-1. The morphological surface exhibited a typical composite in which carbon-silica presents its characteristic stacked tubular shape, and Ti, Zn, Si, C, and O became the primary elements in the two samples. The nitrogen adsorption-desorption curves of TiO_2/CSNs and ZnO/CSNs revealed a combination of types I and IV isotherms, indicating the existence of both micropores and mesopores with the surface area of the impregnated samples decreased due to the blocking pore after impregnation. Moreover, ZnO/CSNs demonstrated a higher degradation percentage against methylene blue than that of TiO_2/CSNs because the active site of Zn^{2+} on the carbon-silica surface that supports the adsorption and direct oxidation of methylene blue on the ZnO surface.

Acknowledgments

This work was financially supported by International Collaboration Grant 2024 from Universitas Sebelas Maret under contract 194.2/UN27.22/PT.01.03/2024.

CRediT Author Statement Author

Author Contributions: M. Ulfa: Conceptualization, Investigation, Resources, Data Curation, Writing, Review and Editing, Supervision; M. Ulfa and I. U. Hasanah Methodology, Formal Analysis, Data Curation, Writing Draft Preparation; M. Ulfa and I. U. Hasanah and I. Setiarini : Review and Editing, Data Curation, and Validation. All authors have read and agreed to the published version of the manuscript.

References

[1] Ulfa, M., Nur, C., Amalia, N. (2023). Fine-tuning mesoporous silica properties by a dual-template ratio as TiO_2 support for dye photodegradation booster. *Heliyon*, 9(6), e16275. DOI: 10.1016/j.heliyon.2023.e16275.

[2] Essa, W.K., Yasin, S.A., Abdullah, A.H., Thalji, M.R., Saeed, I.A., Assiri, M.A., Chong, K.F., Ali, G.A.M. (2022). Polyethylene Terephthalate Nanofiber-Multi-Walled Carbon Nanotube Composite. *Water*, 25, DOI: 10.3390/w14081242.

[3] Safri, A., Fletcher, A.J. (2022). Effective Carbon/TiO_2 Gel for Enhanced Adsorption and Demonstrable Visible Light Driven Photocatalytic Performance. *Gels*, 8(4) DOI: 10.3390/gels8040215.

[4] Chen, B., Zhang, X., Zhang, X., Lin, Q. (2020). Facile preparation of ultrathin-wall graphitic mesoporous carbon containing graphene sheets with desirable adsorption performance for organic dyes. *Journal of Molecular Liquids*, 319, 114306. DOI: 10.1016/j.molliq.2020.114306.

[5] Gao, Z.Z., Qi, N., Chen, W.J., Zhao, H. (2022). Construction of hydroxyethyl cellulose/silica/graphitic carbon nitride solid foam for adsorption and photocatalytic degradation of dyes. *Arabian Journal of Chemistry*, 15 (9), 1-16. DOI: 10.1016/j.arabjc.2022.104105.

[6] Prasetyoko, D., Sholeha, N.A., Subagyo, R., Ulfa, M., Bahruji, H., Holilah, H., Pradipta, M.F., Jalil, A.A. (2023). Mesoporous ZnO nanoparticles using gelatin - Pluronic F127 as a double colloidal system for methylene blue photodegradation. *Korean, J. Chem. Eng.* 40(1), 112–123. DOI: 10.1007/s11814-022-1224-y.

[7] Ulfa, M., Pangestuti, I., Anggreani, C.N. (2024). Physicochemical Characteristics of Titania Particles Synthesized with Gelatin as a Template Before and After Regeneration and Their Performance in Photocatalytic Methylene Blue. *Bulletin of Chemical Reaction Engineering & Catalysis*, 19(2), 242–251. DOI: 10.9767/bcrec.20138.

[8] Chanhom, P., Charoenlap, N., Tomapatanaget, B., Insin, N. (2017). Colloidal titania-silica-iron oxide nanocomposites and the effect from silica thickness on the photocatalytic and bactericidal activities. *Journal of Magnetism and Magnetic Materials*, 427(June), 54–59. DOI: 10.1016/j.jmmm.2016.10.123.

[9] Cani, D., Waal, J.C. Van Der, Pescarmona, P.P. (2021). Highly accessible, doped TiO_2 nanoparticles embedded at the surface of SiO_2 as photocatalysts for the degradation of pollutants under visible and UV radiation. *Applied Catalysis A: General*, 621(April), 118179. DOI: 10.1016/j.apcata.2021.118179.

[10] Vasu, P., Reddy, G., Rajendra, B., Reddy, P., Venkata, M., Reddy, K., Raghava, K., Shetti, N.P., Saleh, T.A., Aminabhavi, T.M. (2020). A review on multicomponent reactions catalysed by zero-dimensional / one-dimensional titanium dioxide (TiO_2) nanomaterials : Promising green methodologies in organic chemistry. *Journal of Environmental Management*, 279, 111603. DOI: 10.1016/j.jenvman.2020.111603.

[11] Albiss, B., Abu-Dalo, M. (2021). Photocatalytic degradation of methylene blue using zinc oxide nanorods grown on activated carbon fibers. *Sustainability (Switzerland)*, 13(9) DOI: 10.3390/su13094729.

[12] Li, J., Han, L., Zhang, T., Qu, C., Yu, T., Yang, B. (2022). Removal of Methylene Blue by Metal Oxides Supported by Oily Sludge Pyrolysis Residues. *Applied Sciences (Switzerland)*, 12(9) DOI: 10.3390/app12094725.

[13] Barakat, M.A., Kumar, R., Eniola, J.O. (2021). Adsorption and photocatalytic scavenging of 2-chlorophenol using carbon nitride-titania nanotubes based nanocomposite: Experimental data, kinetics and mechanism. *Data in Brief*, 34, 106664. DOI: 10.1016/j.dib.2020.106664.

[14] Raizada, P., Soni, V., Kumar, A., Singh, P., Parwaz Khan, A.A., Asiri, A.M., Thakur, V.K., Nguyen, V.H. (2021). Surface defect engineering of metal oxides photocatalyst for energy application and water treatment. *Journal of Materiomics*, 7 (10), 1-17, DOI 10.1016/j.jmat.2020.10.009.

[15] Waghchaure, R.H., Adole, V.A., Jagdale, B.S. (2022). Photocatalytic degradation of methylene blue, rhodamine B, methyl orange and Eriochrome black T dyes by modified ZnO nanocatalysts: A concise review. *Inorganic Chemistry Communications*, 143 (109764), 1–15. DOI: 10.1016/j.inoche.2022.109764.

[16] Li, X., Zhang, L. (2022). Adsorption of Methylene Blue on TiO_2/SiO_2 Prepared by Chemical Vapor Deposition. *Russian Journal of Physical Chemistry A*, 96(6), 1304–1313. DOI: 10.1134/S0036024422060309.

[17] Ulfa, M., Al Afif, H., Saraswati, T.E., Bahruji, H. (2022). Fast Removal of Methylene Blue via Adsorption-Photodegradation on TiO_2/SBA-15 Synthesized by Slow Calcination. *Materials*, 15(16), 1–13. DOI: 10.3390/ma15165471.

[18] Assaker, K., Carteret, C., Stébé, M.J., Blin, J.L. (2014). Multi-techniques investigation of mesoporous zinc and tungsten titanates materials. *Microporous and Mesoporous Materials*, 194, 208–218. DOI: 10.1016/j.micromeso.2014.03.044.

[19] Gholami, P., Khataee, A., Ritala, M. (2022). Template-free hierarchical trimetallic oxide photocatalyst derived from organically modified ZnCuCo layered double hydroxide. *Journal of Cleaner Production*, 366(February), 132761. DOI: 10.1016/j.jclepro.2022.132761.

[20] Zawrah, M.F., Alhogbi, B.G. (2021). Preparation and characterization of SiO_2@C nanocomposites from rice husk for removal of heavy metals from aqueous solution. *Ceramics International*, 47(16), 23240–23248. DOI: 10.1016/j.ceramint.2021.05.036.

[21] Chandrasekar, G., Son, W.J., Ahn, W.S. (2009). Synthesis of mesoporous materials SBA-15 and CMK-3 from fly ash and their application for CO_2 adsorption. *J. Porous Mater*. 16, 545-551. DOI: 10.1007/s10934-008-9231-x

[22] Guo, R., Guo, J., Yu, F., Gang, D.D. (2013). Synthesis and surface functional group modifications of ordered mesoporous carbons for resorcinol removal. *Microporous and Mesoporous Materials*, 175, 141–146. DOI: 10.1016/j.micromeso.2013.03.028.

[23] Sevilla, M., Fuertes, A.B. (2006). Catalytic graphitization of templated mesoporous carbons. *Carbon*, 44(3), 468–474. DOI: 10.1016/j.carbon.2005.08.019.

[24] Leyva-García, S., Lozano-Castelló, D., Morallón, E., Cazorla-Amorós, D. (2016). Silica-templated ordered mesoporous carbon thin films as electrodes for micro-capacitors. *Journal of Materials Chemistry A*, 4(12), 4570–4579. DOI: 10.1039/c5ta10552h.

[25] Zhao, W., Zhang, H., He, Q., Han, L., Wang, T., Guo, F., Wang, W. (2022). Controllable synthesis of porous silicate@carbon heterogeneous composite from Coal Gangue waste as eco-friendly superior scavenger of dyes. *Journal of Cleaner Production*, 363 (October 2021), 132466. DOI: 10.1016/j.jclepro.2022.132466.

[26] Ulfa, M., Prasetyoko, D., Mahadi, A.H., Bahruji, H. (2020). Size tunable mesoporous carbon microspheres using Pluronic F127 and gelatin as co-template for removal of ibuprofen. *Science of the Total Environment*, 711, 135066. DOI: 10.1016/j.scitotenv.2019.135066.

[27] Ulfa, M., Pertiwi, Y.E., Saraswati, T.E., Bahruji, H., Holilah, H. (2023). Synthesis of iron triad metals-modified graphitic mesoporous carbon for methylene blue photodegradation. *South African Journal of Chemical Engineering*, 45 (May), 149–161. DOI: 10.1016/j.sajce.2023.05.008.

[28] Xu, X., Wang, H., Xie, Y., Liu, J., Yan, H., Liu, W. (2018). Graphitized Mesoporous Carbon Derived from ZIF-8 for Suppressing Sulfation in Lead Acid Battery and Dendritic Lithium Formation in Lithium Ion Battery. *Journal of The Electrochemical Society*, 165(13), A2978–A2984. DOI: 10.1149/2.0361813jes.

[29] Induchoodan, G., Jansson, H., Swenson, J. (2021). Influence of graphene oxide on asphaltene nanoaggregates. *Colloids Surfaces A Physicochem. Eng. Asp*. 630, 630, 127614, 1-13, DOI: 10.1016/j.colsurfa.2021.127614

[30] Buscarino, G., Vaccaro, G., Agnello, S., Gelardi, F.M. (2009). Variability of the Si-O-Si angle in amorphous-SiO_2 probed by electron paramagnetic resonance and Raman spectroscopy. *Journal of Non-Crystalline Solids*, 355(18–21), 1092–1094. DOI: 10.1016/j.jnoncrysol.2008.12.017.

[31] Rueda-Márquez, J.J., Palacios-Villarreal, C., Manzano, M., Blanco, E., Ramírez del Solar, M., Levchuk, I. (2020). Photocatalytic degradation of pharmaceutically active compounds (PhACs) in urban wastewater treatment plants effluents under controlled and natural solar irradiation using immobilized TiO_2. *Solar Energy*, 208(August), 480–492. DOI: 10.1016/j.solener.2020.08.028.

[32] Ediati, R., Ulfa, M., Fansuri, H., Ramli, Z., Nur, H. (2014). Influence of $TiOO_2$/TS-1 Calcination on Hydroxylation of Phenol. *J. Fund. Math, Sci.* 46(1), 76–90. DOI: 10.5614/j.math.fund.sci.2014.46.1.7.

[33] Maimunawaro, Rahman, S.K., Rampun, E.L.A., Rahma, A., Elma, M. (2020). Deconvolution of carbon silica templated thin film using ES40 and P123 via rapid thermal processing method. *Materials Today: Proceedings*, 31, 75–78. DOI: 10.1016/j.matpr.2020.01.195.

[34] Awadh, S.M., Yaseen, Z.M. (2019). Investigation of silica polymorphs stratified in siliceous geode using FTIR and XRD methods. *Materials Chemistry and Physics*, 228 (February), 45–50. DOI: 10.1016/j.matchemphys.2019.02.048.

[35] Stobinski, L., Lesiak, B., Malolepszy, A., Mazurkiewicz, M., Mierzwa, B., Zemek, J., Jiricek, P., Bieloshapka, I. (2014). Graphene oxide and reduced graphene oxide studied by the XRD, TEM and electron spectroscopy methods. *Journal of Electron Spectroscopy and Related Phenomena*, 195, 145–154. DOI: 10.1016/j.elspec.2014.07.003.

[36] Luan, Z., Fournier, J.A. (2005). In situ FTIR spectroscopic investigation of active sites and adsorbate interactions in mesoporous aluminosilicate SBA-15 molecular sieves. *Microporous and Mesoporous Materials*, 79(1–3), 235–240. DOI: 10.1016/j.micromeso.2004.11.012.

[37] Sapawe, N., Ariff Rustam, M., Hafizan Hakimin Mahadzir, M., Kamal Ezzat Mohamad Lani, M., Raidin, A., Farhan Hanafi, M. (2019). A Novel Approach of In-Situ Electrobiosynthesis of Metal Oxide Nanoparticles Using Crude Plant Extract as Main Medium for Supporting Electrolyte. *Materials Today: Proceedings*, 19, 1441–1445. DOI: 10.1016/j.matpr.2019.11.166.

[38] Qaseem, S., Dlamini, D.S., Zikalala, S.A., Tesha, J.M., Husain, M.D., Wang, C., Jiang, Y., Wei, X., Vilakati, G.D., Li, J. (2020). Electro-catalytic membrane anode for dye removal from wastewater. *Colloids and Surfaces A: Physicochemical and Engineering Aspects*, 603 (February), 125270. DOI: 10.1016/j.colsurfa.2020.125270.

[39] Shilpa, G., Mohan Kumar, P., Kishore Kumar, D., Deepthi, P.R., Sukhdev, A., Bhaskar, P. (2022). A rutile phase-TiO_2 film via a facile hydrothermal method for photocatalytic methylene blue dye decolourization. *Materials Today: Proceedings*, 62, 5477–5482. DOI: 10.1016/j.matpr.2022.04.148.

[40] Liu, X., Wang, G., Zhi, H., Dong, J., Hao, J., Zhang, X., Wang, J., Li, D., Liu, B. (2022). Synthesis of the Porous ZnO Nanosheets and TiO_2/ZnO/FTO Composite Films by a Low-Temperature Hydrothermal Method and Their Applications in Photocatalysis and Electrochromism. *Coatings*, 12(5) DOI: 10.3390/coatings12050695.

[41] Wu, M., Shi, L., Lim, T.T., Veksha, A., Yu, F., Fan, H., Mi, J. (2018). Ordered mesoporous Zn-based supported sorbent synthesized by a new method for high-efficiency desulfurization of hot coal gas. *Chemical Engineering Journal*, 353(July), 273–287. DOI: 10.1016/j.cej.2018.07.134.

[42] Saad, A.M., Abukhadra, M.R., Abdel-Kader Ahmed, S., Elzanaty, A.M., Mady, A.H., Betiha, M.A., Shim, J.J., Rabie, A.M. (2020). Photocatalytic degradation of malachite green dye using chitosan supported ZnO and Ce–ZnO nano-flowers under visible light. *Journal of Environmental Management*, 258, 110043. DOI: 10.1016/j.jenvman.2019.110043.

[43] Jayanthi Kalaivani, G., Suja, S.K. (2016). TiO_2 (rutile) embedded inulin - A versatile bio-nanocomposite for photocatalytic degradation of methylene blue. *Carbohydrate Polymers*, 143, 51–60. DOI: 10.1016/j.carbpol.2016.01.054.

[44] Fatimah, I., Prakoso, N.I., Sahroni, I., Musawwa, M.M., Sim, Y.L., Kooli, F., Muraza, O. (2019). Physicochemical characteristics and photocatalytic performance of TiO_2/SiO_2 catalyst synthesized using biogenic silica from bamboo leaves. *Heliyon*, 5(11), e02766. DOI: 10.1016/j.heliyon.2019.e02766.

[45] Wang, Y., Lu, Y., Luo, R., Zhang, Y., Guo, Y., Yu, Q., Liu, X., Kim, J.K., Luo, Y. (2018). Densely-stacked N-doped mesoporous TiO_2/carbon microsphere derived from outdated milk as high-performance electrode material for energy storages. *Ceramics International*, 44(14), 16265–16272. DOI: 10.1016/j.ceramint.2018.06.020.